Energetic Impact of Reconstructed Debris Flow on the Intensity and Duration of Growth Disturbances of Tree Rings by Numerical Simulation and Remote Sensing

Xueliang Wang *, Juanjuan Sun, Yong Zhang, Qisong Jiao, Shengwen Qi, Ran Wang, Haiyang Liu, Mengjie Zhang

Posted Date: 31 May 2023

doi: 10.20944/preprints202305.2181.v1

Keywords: debris flow simulation; remote sensing; tree ring; Massflow; northeastern Tibet

Article

Energetic Impact of Reconstructed Debris Flow on the Intensity and Duration of Growth Disturbances of Tree Rings by Numerical Simulation and Remote Sensing

Xueliang Wang [1,2,3,*], Juanjuan Sun [1,2,3], Yong Zhang [4], Qisong Jiao [5], Shengwen Qi [1,2,3], Ran Wang [6], Haiyang Liu [7] and Mengjie Zhang [1,2,3]

[1] Key Laboratory of Shale Gas and Geoengineering, Institute of Geology and Geophysics, Chinese Academy of Sciences, Beijing 100029, China
[2] Innovation Academy for Earth Sciences, CAS, Beijing 100029, China
[3] University of Chinese Academy of Sciences, Beijing 100049, China
[4] Key Laboratory of Land Surface Pattern and Simulation, Institute of Geographic Sciences and Natural Resources Research, Chinese Academy of Sciences, Beijing, 100101, China
[5] National Institute of Natural Hazards, MEMC, Beijing 100085, China
[6] Research Center of Applied Geology of China Geological Survey, Chengdu 610036, China
[7] China Aero Geophysical Survey and Remote Sensing Center For Natural Resources, Beijing 100083, China
* Correspondence: wangxueliang@mail.iggcas.ac.cn

Abstract: Rare study on quantitative relationship between energetic impact of debris flows on the intensity and duration of growth disturbances of tree rings was carried out, partly due to lack of feasible approaches and detailed field evidence. In this study, we firstly determine the age of a recent debris flow derived from historic landslide deposits at Qingyang mountain (QYM) on the northeastern Tibet plateau by dendrogeomorphic technique. We acquired the quantitative data of annual widths of tree rings in history and confirmed the influence of debris flow rather than other factors (e.g. climatic event and inset outbreaking) in disturbing the growth of tree rings in a specific year. Using the approach, we determined the age of the debris flow at QYM occurred in 1982, which was speculated to be triggered by high monthly precipitation of July in 1982. Subsequently, based on the boundaries of historic debris flow identified on remote sensing images before and after 1982 and depth-integrated continuum model, we reconstructed the process of 1982-debris flow and obtained the kinematic energy of debris flow impacting on the sampled trees. Based on the study, we observed that two growth disturbance patterns of tree rings influenced by the reconstructed 1982-debris flow were revealed including growth suppression and asymmetric growth. A raw logarithm relationship between duration (i.e. lasting time for the disturbed tree rings to recover the initial width) and intensity of growth disturbances (i.e. growth suppression ratio of disturbed tree rings) was obtained. We concluded that there is a negative exponential relationship between simulated kinematic energy of debris flow impacting on the disturbed trees and time to recover the initial width of corresponding tree rings.

Keywords: debris flow simulation; remote sensing; tree ring; Massflow; northeastern Tibet

1. Introduction

Different kinematic energy of debris flow impacting on trees can lead to different failure characteristics and growth disturbances [1]. Previous studies dominantly focused on the relationships of kinematic energy of rockfall with morphological characteristics of trees (e.g. diameter at breast height and stand density) [2–4]. Rare study on quantitative relationship between impacting of debris flows and the intensity and duration of growth disturbances of tree rings was carried out. Firstly, large amounts of tree ring samples disturbed by the same debris flow event are needed, but

 doi:10.20944/preprints202305.2181.v1

it is difficult for many trees to preserve well on site in a long history. Secondly, the criterion to quantify the growth suppression or other disturbed characteristics in tree ring of different tree species influenced by debris flow is still limited for building the relationship. The last and the most difficult one is how to monitor or acquire the kinematic energy of debris flow impacting on different disturbed trees.

Although new geochronological methods increase the number of dated geo-hazards (e.g. landslide and debris flow), absolute dating methods (e.g. Cosmic Ray Exposure, Optically Stimulated Luminescence, Thermoluminescence and Uranium-series (234U/230Th) dating) are still less developed for geo-hazards occurred on the timescale of centennial or millennial [5,6]. Dendrogeomorphic technique (tree ring-based) has been developed to constrain the ages of geo-hazards on centennial or millennial scale that were recorded as the growth disturbance in tree rings [7–11]. Frequent geo-hazards impact the trees around, leading to the growth disturbance of tree rings (e.g. wider or narrower rings, missing of rings) that were used to determine the time and frequency of geo-hazards [12–16]. However, there are also some other factors, such as earthquake, temperature, precipitation and inset outbreaking, leading to the growth disturbance of tree rings, which make the identification of landslide event complex [16–18]. Meanwhile, random events around a tree like single block hitting and water flowing around tree root could also disturb the growth of tree. Until now, studies of specific characteristics and index values of growth disturbance of tree rings of different tree species influenced by geo-hazards especially debris flows are still limited, impending the timing of debris flows by dendrogeomorphic technique.

With the development of remote sensing, images and Digital Elevation Model (DEM) obtained by satellite technique, Unmanned Aerial Vehicle (UAV) and terrestrial lidar system were used to identify debris flows and to analyze the geometric characteristics of debris flows [19–21]. Regional spatial distribution of geo-hazards has been mapped widely using the images obtained by satellite technique [21,22]. One of its obvious merits is that the satellite images provide clear visible evidence of debris flows occurred there during a period. However, because of its strict application conditions (e.g. available satellite, suitable weather conditions and acritical data acquiring setting) for acquiring images, time series of past global satellite images rarely continue yearly or monthly focusing on an area, limiting the application of satellite images for reconstructing the evolution process of geo-hazards.

In previous study, Zhang et al., [16] reconstructed the centennial-scale process activity of landslides at QYM using dendrogeomorphic technique. However, the evidence to define the occurrence of landslide or debris flows solely by dendrogeomorphic technique is not sufficient because of the uncertain complex factors. Hence, in this study, we intend to combine remote sensing with dendrogeomorphic technique to provide the evidence of occurrence of debris flows and to reveal its precise age. After determining the age, we study the specific characteristics and index values of growth disturbance of tree rings (e.g. growth suppression ratio and lasting time for tree rings to recover the normal width) in the year of the debris flows. Furthermore, to reveal the kinematic energy of debris flows impacting on the disturbed trees at QYM and the rarely studied relationship, we try to use numerical simulation of depth-integrated continuum model and remote sensing images to reconstruct evolution process including spatial distribution of kinematic energy of the dated debris flow.

2. Materials and Methods

2.1. Study area and field investigation

QYM is located in the northeastern Qilian Shan range. Because of tectonic faults and long-term weathering, landslides and rockfalls occurred frequently with widely distributed landslide deposits on the mountains (Figure 1). There were small landslides occurred at the middle section of QYM before 1970 [16]. The landslides located at elevations ranging from 3375 to 3450 m a.s.l. (Figure 1b). By the field work, we observed that historical landslide deposits were transformed as the initiation zone of typical debris flow, followed by channel of propagation (with channel depth of ~1.9 m) and

Preprints (www.preprints.org) | NOT PEER-REVIEWED | Posted: 31 May 2023 doi:10.20944/preprints202305.2181.v1

accumulation zone (Figure 1). After the debris flow, a recent smaller one has been growing obviously after 2012 on site (Figure 1a), which partly verifies the dynamic evolution of historic debris flows in the study area. The grain size of the deposits mostly ranges from 0.001–0.04 m^3, which is the small rock blocks class by ISRM (1979) [17]. Based on topographic analysis and filed investigation, the total volume of the deposits of accumulation zone is estimated as 4.9×104 m3, with an average depth of 5.5 m.

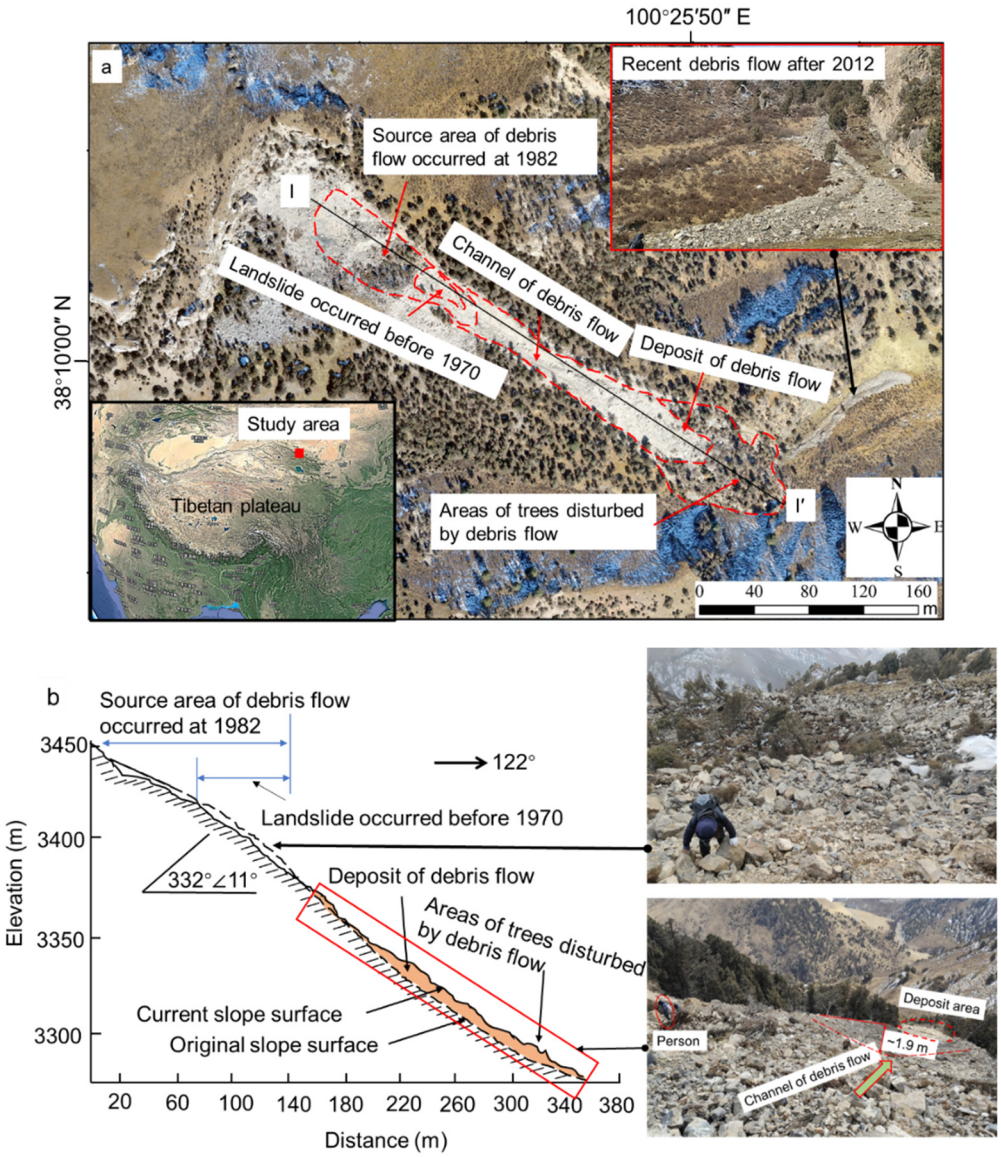

Figure 1. (a) Location of the landslide and debris flow at Qingyang mountain and (b) topographic profile of I-I' in Figure 1(a).

The trees of Qilian junipers mostly grow on sunny slopes at elevations from 3000–3600 m a.s.l. at QYM [17]. The debris flow destroyed some trees grew on the slope. Base on the site work, we noticed that more than 20 trees were hit (i.e. disturbed) by the debris on the accumulation zone, which were demonstrated by tree scars, injuries on the stem and inclined trees on the deposit (Figure 2).

Preprints (www.preprints.org) | NOT PEER-REVIEWED | Posted: 31 May 2023 doi:10.20944/preprints202305.2181.v1

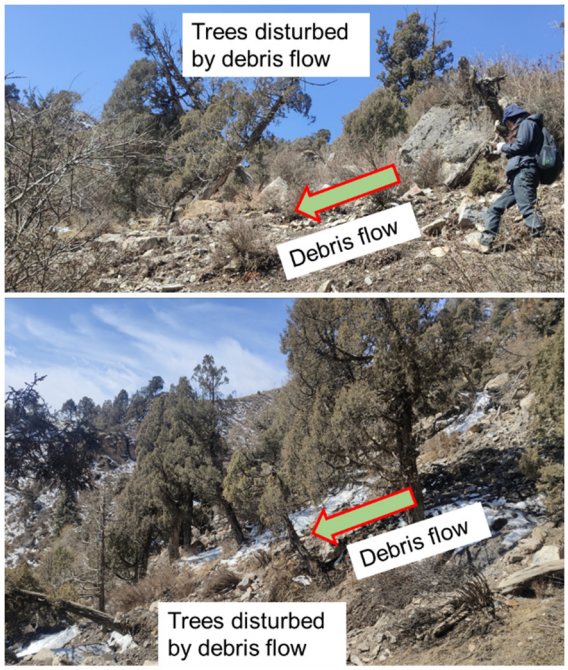

Figure 2. Trees disturbed by debris flow on the accumulation zone at QYM.

2.2. Collecting of satellite images and DEM

We collected a satellite imagery of KH4B satellite (number of DS1108-2184DA088) in 1970 with resolution of 1.8 m (Figure 3a), which was the earliest available one with high quality in the study area. The images in 2012 (Figure 3b) and 2019 (Figure 1a) were obtained from Google Earth and UAV. We obtained 476 photographs taken over an area of about 10 km^2 by UAV in 2019, which was used to create a 0.3-m-resolution DEM. The images and DEM were used to analyze the temporal evolution of landsliding at QYM and to simulate the debris flow as basic data by numerical modelling.

Although the boundaries of landslides and former debris flows occurred before 1970 (i.e. the year of the imagery obtained) on KH4B satellite imagery were difficult to exactly check on site, we could still roughly verify the identification by comparing the white color boundary on the imagery (Figure 3a) and exposure of rock mass on site. In contrast, clear image in 2012 and currently well-preserved boundary and characteristics of deposits on site help us to easily verify the boundary of recent debris flow (Figure 3b).

Preprints (www.preprints.org) | NOT PEER-REVIEWED | Posted: 31 May 2023 doi:10.20944/preprints202305.2181.v1

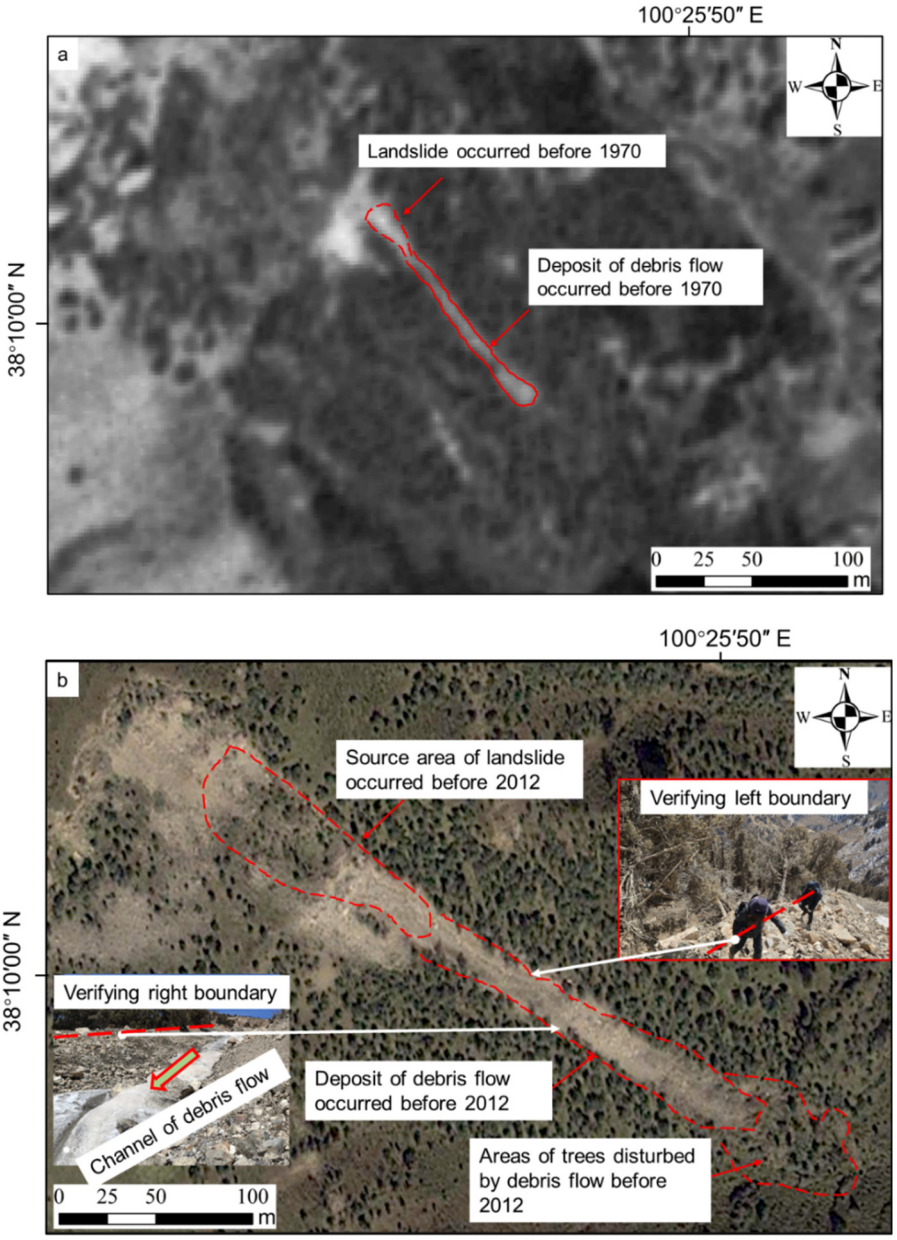

Figure 3. (a) Distribution of the landslide and debris flow occurred before 1970 from an imagery of KH4B satellite in 1970; (b) Distribution of the landslide and debris flow occurred before 2012 from an imagery of Google Earth in 2012. .

2.3. Width measurement of core samples

To collect the core samples of tree rings, we chose the trees with obvious injuries or inclined ones on or near the debris flow deposit. A total of two or three increment cores were extracted per tree using increment borers from two directions including the scar direction (i.e. the direction of debris flowing) and the opposite one [23]. If there are no obvious scars on the trees, we collected cores in the supposed direction of the debris flow movement (i.e., upslope and downslope cores) [9]. We sampled all Qilian junipers on the deposit body with diameters at breast height exceeding 20 cm (the highest of 110 cm) with increment borers. We marked the locations of the core samples on the topographic map created from our 0.3-m-resolution DEM. Ultimately, a total of 52 increment cores were extracted from 23 Qilian juniper trees.

Reference to previous studies [23,24], we dealt with the collected samples in lab based on standard dendrogeomorphical technique. Firstly, the samples were put in the air to make them dry. Secondly, the dry samples were firmed in wood grooves by glue. Thirdly, the firmed samples were

Preprints (www.preprints.org) | NOT PEER-REVIEWED | Posted: 31 May 2023 doi:10.20944/preprints202305.2181.v1

polished using fine sandpaper to make the cells of increment cores clear to observe by microscope. Lastly, we measured the annual widths of tree rings using instrument of LINTAB™ (Figure 3) whose maximum resolution is 1/1,000 mm (http://www.rinntech.de/content/view/16/47/lang,english/index.html). The measured data were automatically recorded by the software platform of TSAP-Win™ for tree ring analyses (http://www.rinntech.de/content/view/17/48/lang,english/index.htm).

After measuring the annual widths of tree rings, we used a previously built reference chronology in the same area for precise cross-dating and age corrections of the core samples disturbed by the debris flow using COFECHA [16,25]. The verification of cross-dating accuracy is based on the value of correlation coefficient between measured annual width of tree rings and reference chronology larger than 0.4 [26].

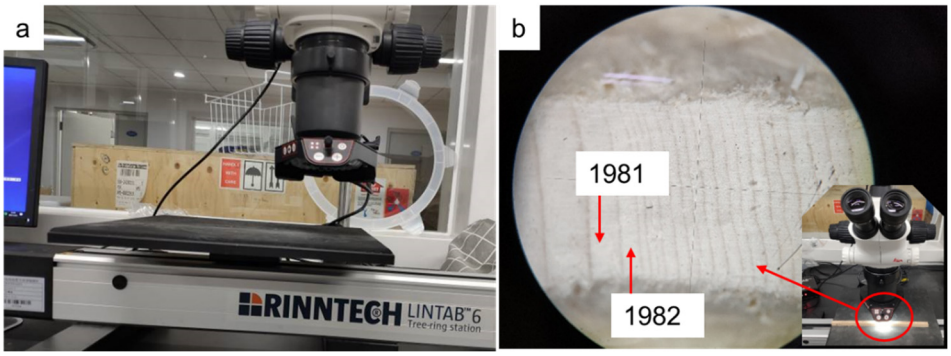

Figure 4. (a) The instrument of LINTAB™-6 used for measuring annual width of tree ring; (b) The image of increment core observed from LINTAB™-6. .

2.4. Numerical simulation of debris flow

Kinematic energy of debris flow was simulated through the numerical approach of Massflow that was used for debris flow dynamic propagation process modelling [27]. The Massflow is based on the depth-integrated continuum model, transforming the 3D description of the dynamic process of debris flow into a simple 2D problem by integrating the Navier–Stokes equations in the depth direction [28]. Under the depth integral condition, Leibniz's law and dynamic boundary conditions were used to simplify the mass and momentum conservation equations as follows [29,30]:

$$\frac{\partial(\bar{\rho}h)}{\partial t}+\frac{\partial(\bar{\rho}h\bar{v}_x)}{\partial x}+\frac{\partial(\bar{\rho}h\bar{v}_y)}{\partial y}=0 \quad (1)$$

$$\frac{\partial(\bar{\rho}h\bar{v}_x)}{\partial t}+\frac{\partial(\beta_{v_xv_x}\bar{\rho}h\bar{v}_x^2)}{\partial x}+\frac{\partial(\beta_{v_xv_y}\bar{\rho}h\bar{v}_x\bar{v}_y)}{\partial y}=\bar{\rho}g_xh-k_{ap}\bar{\rho}g_zh\frac{\partial(h+z_b)}{\partial x}-(\tau_{zx})_b \quad (2)$$

$$\frac{\partial(\bar{\rho}h\bar{v}_y)}{\partial t}+\frac{\partial(\beta_{v_xv_y}\bar{\rho}h\bar{v}_x\bar{v}_y)}{\partial x}+\frac{\partial(\beta_{v_yv_y}\bar{\rho}h\bar{v}_y^2)}{\partial y}=\bar{\rho}g_yh-k_{ap}\bar{\rho}g_zh\frac{\partial(h+z_b)}{\partial y}-(\tau_{zy})_b \quad (3)$$

where ρ is the mass density; h is the flow height; t is the time; β is the momentum distribution coefficient; v_x, v_y represent the components of the velocity vector on the x and y axes, respectively; g_x, g_y, g_z represent the components of the acceleration of gravity on the x, y, and z axes, respectively; and k_{ap} is the lateral earth pressure coefficient. The calculation expression of k_{ap} is presented in Eq. (4), dominantly controlled by the strain rate of the moving material; here, $(\tau_{zy})_b$ and $(\tau_{zx})_b$ are the basal resistance components.

$$k_{ap}=\frac{2}{\cos^2\varphi}\times\left[1\pm\sqrt{1-(1+\tan^2\delta)\cos^2\varphi}\right]-1 \quad (4)$$

where φ and δ represent the internal friction angle and basal friction angle of the moving material, respectively.

The basal friction stress of debris flow is assumed to obey the Coulomb failure criterion (Eq. 5). For the Coulomb friction model available in Massflow, three dominate parameters are needed for

 doi:10.20944/preprints202305.2181.v1

simulation including cohesion, friction angle and pore water pressure parameter. Usually, it is difficult or even impossible in some cases to carry out field test to obtain the values of parameters used for debris flow simulation. Hence, the parameters used in Massflow simulation were commonly obtained from back analysis of historic events [27,30]. Luckily, historic debris flow event at QYM provides us a good chance to back analyze the parameters by optimizing the simulated debris flow characteristics to fit the occurred ones (e.g. the farthest range and depth of debris flow deposit).

$$\tau = c + \rho g h \cdot tan(\psi) \quad (5)$$

where c and ψ are the cohesion and friction angle of the mass, respectively.

Based on the satellite image of 1970, we plotted the boundary of the debris flow occurred once or more times before 1970 (Figure 3a), which was used as the comparable characteristics with the simulated ones for back analysis. To simulate the dynamic propagation process of debris flow by Massflow, the source area and its thickness should be firstly calculated including three dominant steps as follows:

(1) Build the current DEM of the calculation area. We clipped the specific area of DEM for calculation from the whole DEM of QYM obtained before.

(2) Reconstruct the pre-slide topographic lines of the calculation area. Based on the field investigation and satellite image of 1970, we adjusted the current topographic lines according to the contour lines of surrounding terrain to build an approximately original topographic lines before debris flow in ArcMAP.

(3) Create the area and thickness files of debris flow source area. Using the two DEMs of the original and current ones, we created the source area using the tool of grid subtraction in ArcMAP. Hence the area and thickness of source area could be extracted directly.

Using the source area data and given parameters, we carried out the simulation of debris flow in the platform of Massflow.

3. Results

3.1. Age of debris flow

Using the satellite images of 1970 and 2012, we obtained the different boundaries of the debris flows at different stages in ArcGIS. We note that the boundary in 1970 is small, indicating a small debris flow about 6.1×10^3 m^3 occurred at that time or before (Figure 3a). The length and width of the debris flow presented in the image of 2012 are about 288 and 31 m (Figure 3b), both of which are about twice than that of 1970. Hence, a large debris flow occurred during the period from 1970 to 2012. The geometric features of the debris flow after 2012 do not have significant difference (e.g. from debris flow image of 2019 in Figure 1a), indicating relatively stable state of the debris flow body on the whole in the last ten years (i.e. from 2013 to 2022).

Considering the possibility of the debris flow occurred between 1970 and 2012 and its disturbance on annual width of tree rings, we analyzed the variation of annual widths of sampled tree rings with time (Figure 5). We observed that 19 trees with synchronous growth disturbance of tree rings in 1982 that were collected on debris flow deposit. The growth disturbance includes two patterns. One pattern is the growth suppression of width in tree rings, which is demonstrated by 13 trees in 1982 (Figure 5a). Another pattern is asymmetric growth of rings as demonstrated by 6 trees in 1982 (Figure 5b). For the second pattern, two core samples collected on the opposite sides grow almost equally before a sudden disturbance. After the disturbance, one side grows faster or slower, while the other side does not grow synchronously. Hence, the difference of widths on the two opposite sides becomes larger influenced by the disturbance in the second pattern.

Preprints (www.preprints.org) | NOT PEER-REVIEWED | Posted: 31 May 2023 doi:10.20944/preprints202305.2181.v1

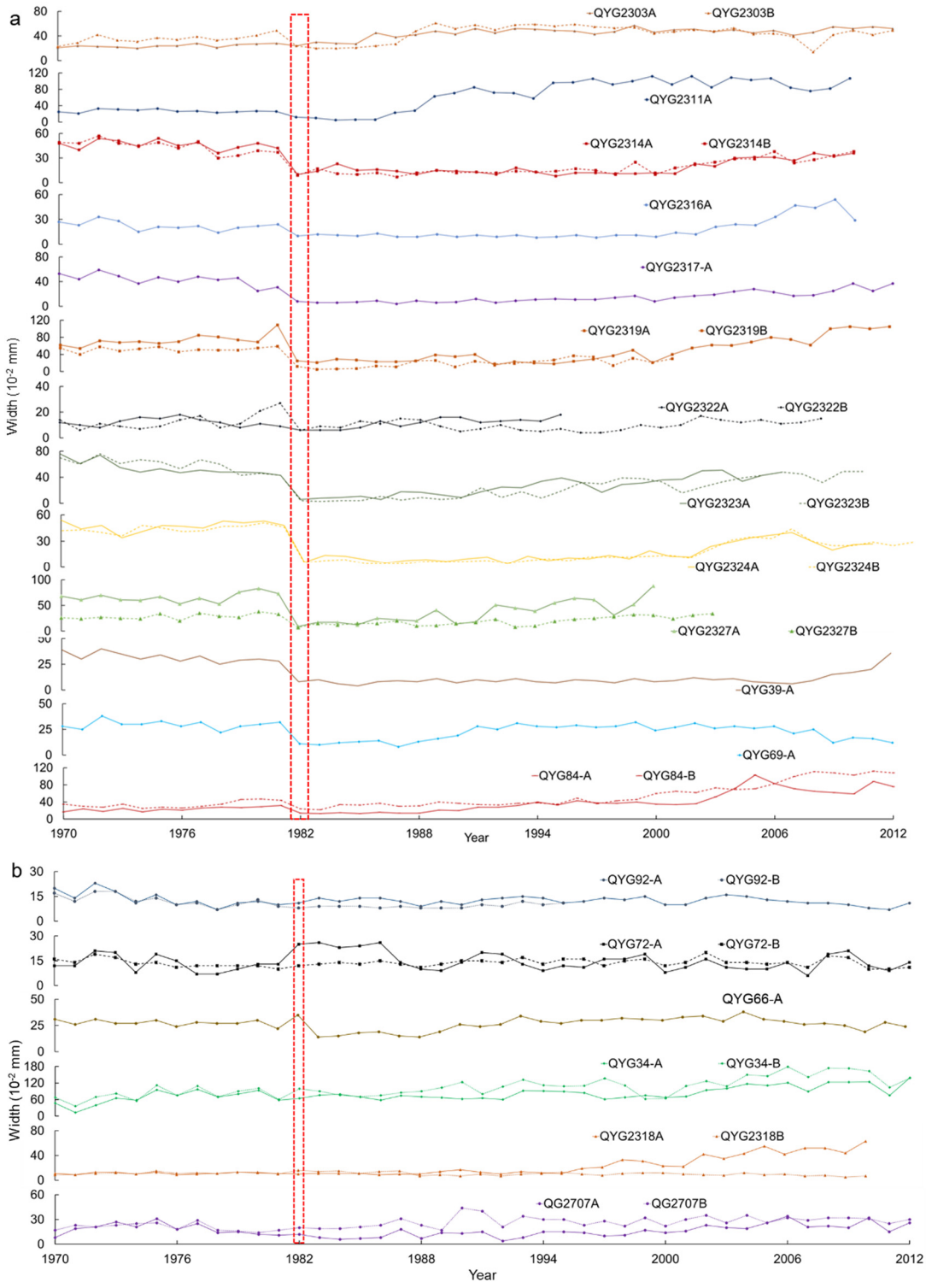

Figure 5. Tree-ring annual widths of sampled Qilian junipers demonstrating growth suppression (a) and asymmetric growth (b) in 1982 as a result of debris flow (red dotted box).

We note that two patterns of growth disturbance of tree rings including growth suppression and asymmetric growth could be observed not only from 19 trees in 1982 but also from growth disturbances in history of a single tree. For example, the annual widths of tree rings QYG2314A and QYG2314B reveal several significant growth disturbance events (e.g. rockfall or landslide) in 1710 (i.e. asymmetric growth), 1860 (i.e. growth suppression) and 1982 (i.e. growth suppression) (Figure 6a). Meanwhile, the annual widths of tree rings of QYG2324A and QYG2324B reveal growth disturbance events in different years of 1742 (i.e. asymmetric growth) and 1810 (i.e. growth

Preprints (www.preprints.org) | NOT PEER-REVIEWED | Posted: 31 May 2023 doi:10.20944/preprints202305.2181.v1

suppression) besides the same year of the 1982-lanslide (i.e. growth suppression) (Figure 6b). Hence, besides the synchronous growth disturbance of tree rings by the same large debris flow event, there are also some random growth disturbances of different trees in history. Meanwhile, there are random growth disturbances in some specific tree rings rather than all of them in Figure 5 (e.g. reduction in 2007of QYG2303B and increment in 2000 of QYG2707A). The missing width data of some tree rings (e.g. QYG 2322A after year of 1996, QYG2324A after year of 2000 and QYG2324A after year of 2003) is due to the artificial causes destroying the core samples. We did not note the obvious effect of positions of samples on the patterns of growth disturbance.

Hence, considering the same debris flow event disturbing the growth of trees at the same time, we attribute the synchronous disturbance of width of 32 tree rings in 1982 to a large debris flow. Combing the visible evidence that a debris flow occurred between 1970 and 2012 by satellite images with the data revealed by the synchronous growth disturbance of tree rings in 1982, we determine the age of the debris flow at QYM as 1982.

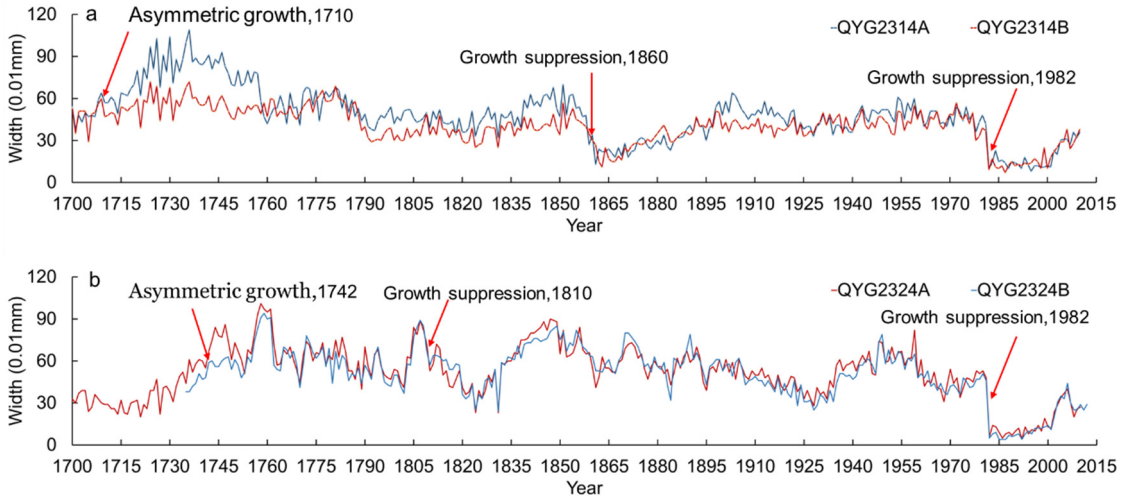

Figure 6. Tree-ring annual widths of sampled Qilian junipers QYG2314(a) and QYG2324(b). Red arrows point to the segments with abnormal growth (growth suppression and asymmetric growth) as a result of landsliding, single block hitting or some others.

3.2. Index values of growth disturbance of tree rings by the 1982-debris flow

By comparing the annual widths of tree rings in 1981 and those in 1982, we calculated the index of growth suppression ratio that equals to width of the disturbed tree rings in the year (i.e. 1982) divides the width of undisturbed ones before the year (i.e. 1981) using the data with obvious growth suppression pattern in our study (Figs. 5a and 7). Meanwhile, previous studies proposed that if the width of tree ring at the year of t is reduced by more than 40% or 50% (i.e. growth suppression ratio in our study) of the width at the year of t-1, and the reduction of width lasts more than 5 years, the year of t is defined as the year of debris flow [16,17]. Similarly, in our study, the maximum growth suppression ratio is 91% (QYG2323B), while the minimum is 51% (QYG2303B), with the average value of 73% (σ =0.16). The lasting time of growth suppression is an important index to reveal the influence of debris flow on growing of tree rings (Van Den Eeckhaut et al. 2009). Based on our data, the lasting time for the disturbed tree rings to recover the initial width by the 1982-debris flow at QYM ranges from 5 to 26 years, with an average of 12 (σ =0.46) years. We observe that the larger the growth suppression ratio influenced by debris flow, the longer the lasting time for tree rings to recover, which is consistent with previous studies [17,31]. Meanwhile, a raw logarithm relationship between lasting time (y) (i.e. time to recover the initial width) and growth suppression ratio (x) ($y=17.56\ln(x)-63.34$, σ =0.32) was obtained in our study (Figure 7).

Preprints (www.preprints.org) | NOT PEER-REVIEWED | Posted: 31 May 2023 doi:10.20944/preprints202305.2181.v1

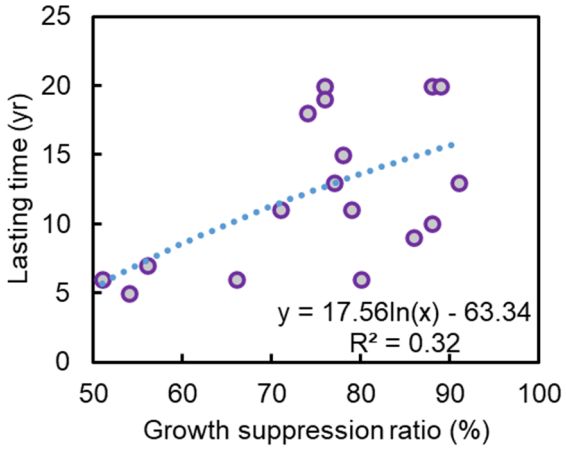

Figure 7. The relation between lasting time and growth suppression ratio of tree rings disturbed by the 1982-debris flow**.**

3.3. Kinematic energy of debris flow impacting on the sampled trees

3.3.1. Parameters obtained by back analysis of the debris flow before 1970

To calibrate the parameters, we simulated the debris flow occurred before 1970 for a series of scenarios with different values of coefficient, friction angle and pore water pressure coefficients. Meanwhile, we collected parameters back analyzed by previous similar studies to make our results more reasonable [27,30,32]. Based on post-debris flow and reconstructed pre-debris flow 1x1 m topography DTMs, ~6130 m^3 of mass was estimated firstly detached from source area (i.e. pre-occurred landslide) before 1970. The results obtained using the cohesion of 8 kPa, the friction coefficient of 0.43 and the pore water pressure coefficient of 0.3 relatively show a good consistency with the farthest range of real debris flow deposit at 1970 (Figure 8).

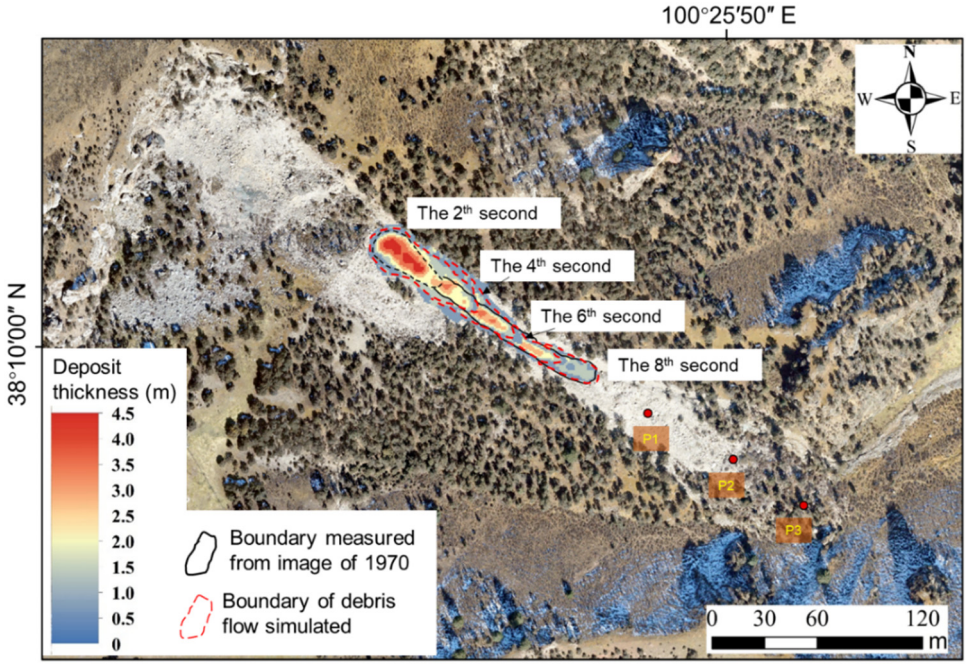

Figure 8. The evolution of debris flow depositing occurred before 1970 by numerical simulation.

 doi:10.20944/preprints202305.2181.v1

The deposit thickness contours of the debris flow before 1970 at times t = 2, 4, 6 and 8 s are shown in Figure 8. Based on the simulated results, we observed that the debris flow moved fast forward from the source area from the beginning to the 4th second. The debris flow material deposited more in the back and front areas than those in the middle area, forming a long-strip shape deposit. From the 4th to the 8th second, the debris flow extended further and finished moving during this second period, controlled by the reduction of material supplying from the source area and the frictional resistance of the deposited material. Eventually, the debris flow deposited as presented in the simulation map of Figure 8 whose farthest range is consistent with the real one in the satellite image of 1970 considering the effect of resolution and shooting angle of satellite image (Figure 3a).

3.3.2. Kinematic energy of the 1982-debris flow impacting on the sampled trees

We simulated the evolution of the 1982-debris flow by Massflow, obtaining the spatial distribution and kinematic energy of debris flow deposit (Figure 9). Because of large amounts of materials detached from the source area, the debris flow transported farther than those before 1970. The debris flow arrived at the top of the current dominant deposit area at the 10th second (Figure 9a). From the 10th to the 14th second, the material started to spread a wider range and reached the area of disturbed trees. From the 14th to the 18th second, the blocks involved in the debris hit the trees (Figure 9b), making them injured, fallen and destroyed. Lastly, the material deposited with final depth of 2~6 m in the front area.

In addition to the deposit depth varying spatially, the impacts are responsible for decreasing the kinematic energy of debris flow. To analyze the energy variation after impacting on the disturbed trees, three monitoring points (Figures 8 and 9b) were set up along the debris flow transport direction during the simulation. The result shows that the kinematic energy was reduced from more than 630.3 KJ (P1) to ~503.4 KJ (P2) before hitting the trees on the debris flow deposit. After hitting the sampled trees, the mass kinematic energy reduced spatially along the runout path, with the largest monitored value of 495.3 KJ located at QYG2323 and the smallest one of 9.1 KJ at QYG2316.

Preprints (www.preprints.org) | NOT PEER-REVIEWED | Posted: 31 May 2023 doi:10.20944/preprints202305.2181.v1

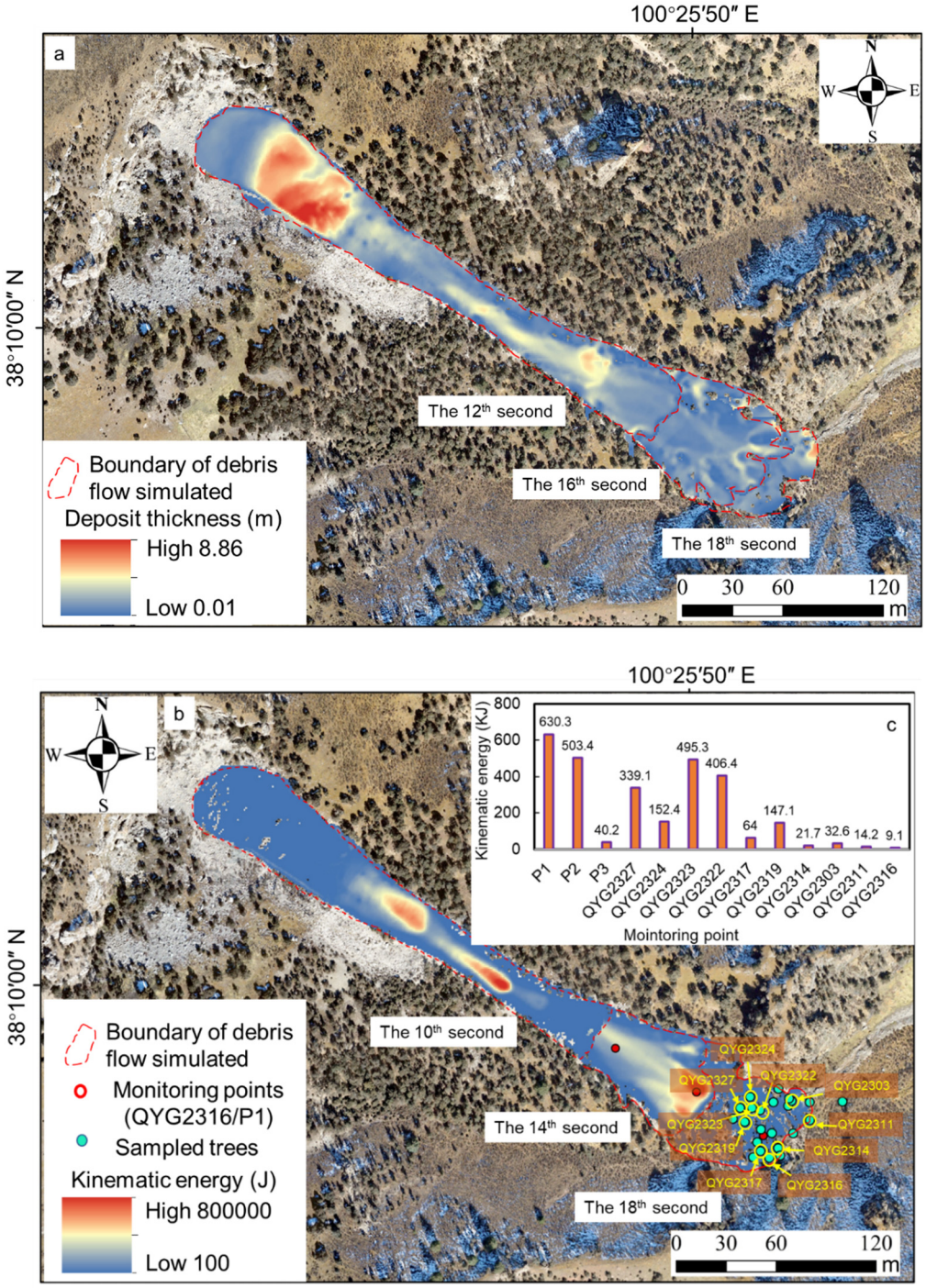

Figure 9. (a) The evolution of debris flow depositing and (b) kinematic energy of debris flow occurred in 1982 by numerical simulation. The locations of monitoring points for kinematic energy of debris flow impacting on the sampled trees (c) were presented in Figure 9b.

4. Discussion

4.1. Effect of precipitation in triggering 1982-debris flow

Precipitation is important in triggering geo-hazards especially debris flow [16,29]. To analyze the effect of precipitation on 1982-debris flow at QYM, we obtained monthly precipitation from 1957 to 1982. We note that precipitation of July is the highest in the whole year averaged by the data of last 25 years (Figure 10a), while the value of July in 1982 (i.e. 1299 mm) is 1.34 times that of average one (i.e. 972 mm). Meanwhile, the monthly precipitation of July in 1982 is the third one in the last 26 years

Preprints (www.preprints.org) | NOT PEER-REVIEWED | Posted: 31 May 2023 doi:10.20944/preprints202305.2181.v1

followed by that of 1981 (i.e. 1374 mm) (Figure 10b). However, we also know that debris flows are commonly triggered by intense short-term precipitation events, sometimes preceded by high antecedent moisture conditions. Hence, because lack of more acute hourly precipitation at QYM, we just speculate that the high monthly precipitation of July in 1982 played an important role in the evolution of 1982-debris flow.

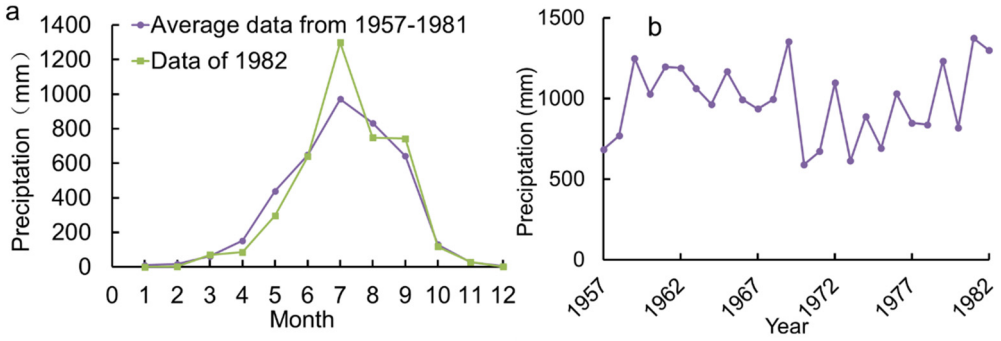

Figure 10. (a) Average monthly precipitation from 1957 to 1981 and monthly data in 1982 around QYM. (b) Monthly precipitation of July from 1957 to 1981 around QYM.

4.2. Relation between impact energy and recover time of disturbed tree rings

It is very important to quantitatively obtain the dynamic growth process of trees (i.e. tree rings) disturbed by debris flows. Based on the relationship, we could predict the possible disturbance degree of trees by a potential debris flows, which provides reference for designing and maintaining bioengineering in debris flows prone areas [33]. Secondly, building the relationship provides us an additional approach to back analyze the evolution process and kinematic energy of historically occurred debris flows using the measurable growth disturbance of tree rings. Hence, based on the data, we attempt to build a relationship between impact kinematic energy of debris flows and time to recover the initial width of tree ring.

Although lack of real record of debris flow process impacting on the sampled trees at QYM, we reconstructed the evolution process including kinematic energy of the 1982-debris flow by numerical simulation. By which, we observed a raw negative exponential function (R^2=0.46) between recover time of disturbed tree rings (y, yr) and kinematic energy of debris flow (x, KJ) larger than 50 KJ at QYM (Figure 11a). It means that higher impact kinematic energy of debris flow leads to larger growth suppression ratio and longer recover time. Meanwhile, we also note that growth suppression ratio almost keeps constant with increasing kinematic energy after reaching the threshold value of ~300 KJ (Figure 11b), which was inferred to the trees were destroyed absolutely without more records of tree rings after that energy.

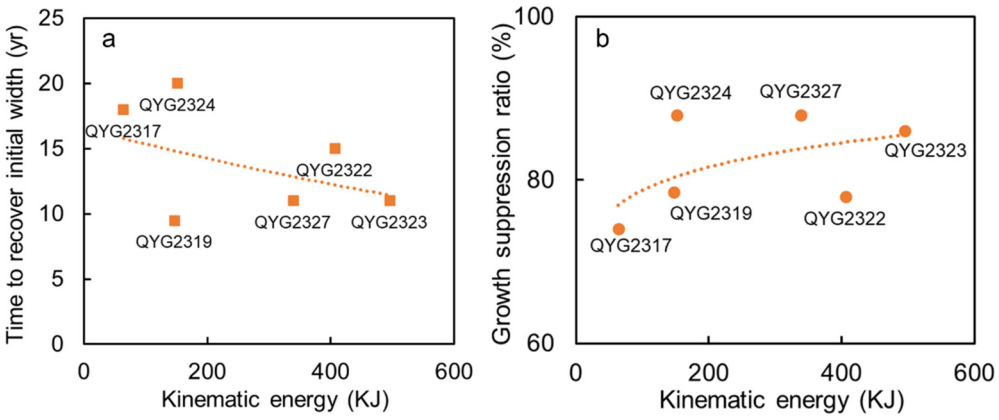

Figure 11. The relations between recover time of disturbed tree rings (a) and the growth suppression ratio (b) and kinematic energy of debris flow (KJ) impacting on the disturbed trees.

 doi:10.20944/preprints202305.2181.v1

4.3. Uncertainty analysis

It is normal for tree rings to have one random growth disturbance pattern (growth suppression or asymmetric growth) influenced by water flow destroying the root systems or even local inset outbreaking, rather than synchronous two patterns of growth disturbance as those influenced by the 1982-debris flow [16–18]. Meanwhile, the influence of climatic events on growth disturbance of tree rings should cover all the local trees rather than only the trees on the debris flow body. Hence, combing with satellite images, the growth disturbance of trees on the debris flow deposit from 1970 to 2012 was used to identify the debris flow occurred in 1982. The disturbance of 19 trees in 1982 was attributed to the relatively large debris flow. Considering several random growth disturbances occurred in specific years (i.e. the years of 1710 and 1860 in QYG2314 in contrast to the years of 1742 and 1810 in QYG2324) (Figure 6) and their similar characteristics with those of 1982 (Figure 5), we suppose that the hitting of small blocks on the trees (or so-called rockfall) probably played an important role in those random disturbances because of no large debris flow observed around the sampled trees from the satellite image of 1970. However, we note that there are some other random growth disturbances without typically identified characteristics in the sampled trees (e.g. 32 tree rings from 1970 to 2012 in Figure 5 and some unlabeled in Figure 6). We do not have enough confidence to attribute all of the growth disturbance events to rockfalls or landslides, instead of the fact possibly demonstrating that complex factors control the growth disturbance of tree rings in natural slopes [16–18]. Research on the characteristics of growth disturbance controlled by different factors (e.g. geo-hazard, climatic forcing or insect outbreaking) is a worthwhile future endeavor.

Our main objective in the study of relationship between kinematic energy and time to recover the initial width of disturbed tree rings was to reveal the possible pattern of the function. Possible errors in the relationship dominate uncertainties in our numerical simulation of debris flow because we lacked precise topography data before 1982 that significantly controls the simulation results of debris flow. We tried to reduce the uncertainty by checking the 1970-satellite image and adjusting the current high resolution DEM data from the surrounding terrains based on our previous experience [30]. Also, the errors due to uncertainties in debris flow simulation likely have more influence on the specific exponent value than the relationship pattern of negative power function (Figure 11a). Accordingly, the degree of uncertainty in the numerical simulation of debris flow does not alter our conclusions about the possible coupling pattern of growth disturbance of tree rings and kinematic energy of debris flow. Bedside, because it is difficult to obtain sufficient data of disturbed tree rings to build a more convinced relationship, the negative power function obtained in this study is raw. It means the relationship is full of so-called epistemic uncertainty comparing with the real one [34]. Hence, field test of debris flow impacting on the trees and long-term monitoring of growth disturbance of tree rings are needed to build a more reliable relationship to revise the conclusion in our study in the future.

5. Conclusions

In this study, we identified the debris flow at QYM occurred in 1982 on the northeastern Tibet by dendrogeomorphic technique and evidence of occurrence on remote sensing images, which was applied to. Using clear boundary of debris flow on remote sensing images before and after 1982 and depth-integrated continuum model, we reconstructed the process of 1982-debris flow and obtained the kinematic energy of debris flow.

1. We observed two growth disturbance patterns of tree rings influenced by the 1982-debris flow including growth suppression and asymmetric growth. By quantitative measurement of annual widths of tree rings in 1981 and 1982 from Qilian junipers, the maximum growth suppression ratio of tree rings influenced by the 1982-debris flow is 91%, while the minimum is 51%, with average value of 73% (σ=0.16). The lasting time for disturbed tree rings by the 1982-debris flow to recover initial width is from 5 to 26 years, with an average of 12 (σ=0.46) years.

2. Using simulated kinematic energy of the 1982-debris flow impacting on the sampled trees, we obtained a raw negative exponential relationship between kinematic energy of debris flow and time to recover the initial width of disturbed tree rings. The negative exponential relationship could be

used to roughly estimate the time for specific trees to recover the initial state after an energy-calculated debris flow hazard.

Author Contribution: Conceptualization, X.W.; methodology X.W., R.W. and Y.Z.; formal analysis, X.W., R. W and J.S.; Investigation, X.W., R.W., J.S., Q.J. and H.L.; writing—original draft preparation, X.W. and J.S.; writing—review and editing, X.W., Y. Z. and S.Q.; visualization, Q.J. and M.Z.; supervision, S.Q.; project administration, X.W. and S.Q.; funding acquisition, X.W. and S.Q. All authors have read and agreed to the published version of the manuscript.

Funding: This work was supported by the Strategic Priority Research Program of the Chinese Academy of Sciences (Grant No. XDA23090402), the China Natural Science Foundation (Grant No. 42172304), and the Second Tibetan Plateau Scientific Expedition and Research Program (STEP) (Grant No. 2019QZKK0904).

Data Availability Statement: The data presented in this study are available on request from the corresponding author.

Acknowledgments: We thank Wenling An and Chenxi Xu for the help of dendrogeomorphic technique.

Competing interests: The authors declare no competing interests.

References

1. Wistuba M, Malik I, Gärtner H, Kojs P, Owczarek P (2013) Application of eccentric growth of trees as a tool for landslide analyses: The example of Picea abies Karst. in the Carpathian and Sudeten Mountains (Central Europe). Catena111:41-55. https://doi.org/10.1016/j.catena.2013.06.027
2. Dorren LKA, Berger F (2006) Stem breakage of trees and energy dissipation during rockfall impacts. Tree Physiol 26:63–71. https://doi.org/10.1093/treephys/26.1.63
3. Perret S, Dolf F, Kienholz H (2004) Rockfalls into forests: Analysis and simulation of rockfall trajectories ? considerations with respect to mountainous forests in Switzerland. Landslides 1(2): 123–130. https://doi.org/10.1007/s10346-004-0014-4
4. Woltjer M, Rammer W, Brauner M, Seidl R, Mohren GMJ, Lexer MJ (2008) Coupling a 3D patch model and a rockfall module to assess rockfall protection in mountain forests. J Environ Manage 87:373–388. https://doi.org/10.1016/j.jenvman.2007.01.031
5. Crosta GB, Clague JJ (2009) Dating, triggering, modelling, and hazard assessment of large landslides. Geomorphology 103:1–4. https://doi.org/10.1016/j.geomorph.2008.04.007
6. Pánek T (2015) Recent progress in landslide dating. Progress in Physical Geography: Earth and Environment 39:168–198. https://doi.org/10.1177/0309133314550671
7. Butler DR, Oelfke JG, Oelfke LA (1986) Historic Rockfall Avalanches, Northeastern Glacier National Park, Montana, U.S.A. Mountain Research and Development 6:261. https://doi.org/10.2307/3673396
8. Šilhán K, Prokešová R, Medveďová A, Tichavský R (2016) The effectiveness of dendrogeomorphic methods for reconstruction of past spatio-temporal landslide behaviour CATENA 147:325–333. https://doi.org/10.1016/j.catena.2016.07.035
9. Stoffel M, Schneuwly D, Bollschweiler M, Lièvre I, Delaloye R, Myint M, Monbaron M (2005) Analyzing rockfall activity (1600–2002) in a protection forest—a case study using dendrogeomorphology. Geomorphology 68:224–241. https://doi.org/10.1016/j.geomorph.2004.11.017
10. Stoffel M (2006) A Review of Studies Dealing with Tree Rings and Rockfall Activity: The Role of Dendrogeomorphology in Natural Hazard Research. Nat Hazards 39:51–70. https://doi.org/10.1007/s11069-005-2961-z
11. Noguchi K, Tsou C-Y, Ishikawa Y, Higaki D, Wu, C-Y (2021) Tree-Ring Based Chronology of Landslides in the Shirakami Mountains, Japan. Water, 13,1185. https://doi.org/10.3390/w13091185
12. Lopez Saez J, Corona C, Stoffel M, Astrade L, Berger F, Malet J-P (2012) Dendrogeomorphic reconstruction of past landslide reactivation with seasonal precision: the Bois Noir landslide, southeast French Alps. Landslides 9:189–203. https://doi.org/10.1007/s10346-011-0284-6
13. Schneuwly DM, Stoffel M (2008) Spatial analysis of rockfall activity, bounce heights and geomorphic changes over the last 50 years – A case study using dendrogeomorphology. Geomorphology 102:522–531. https://doi.org/10.1016/j.geomorph.2008.05.043
14. Šilhán K (2017) Evaluation of growth disturbances of Picea abies (L.) Karst. to disturbances caused by landslide movements. Geomorphology 276:51–58. https://doi.org/10.1016/j.geomorph.2016.10.005

15. Šilhán K (2021) A new tree-ring-based index for the expression of spatial landslide activity and the assessment of landslide hazards. Geomatics, Natural Hazards and Risk 12(1):3409-3428. https://doi.org/10.1080/19475705.2021.2011790
16. Zhang Y, Stoffel M, Liang E, Guillet S, Shao X (2019) Centennial-scale process activity in a complex landslide body in the Qilian Mountains, northeast Tibetan Plateau, China. CATENA 179:29–38. https://doi.org/10.1016/j.catena.2019.03.036
17. Carrara PE, O'Neill JM (2003) Tree-ring dated landslide movements and their relationship to seismic events in southwestern Montana, USA. Quat. res. 59:25–35. https://doi.org/10.1016/S0033-5894(02)00010-8
18. Ciervo F, Rianna G, Mercogliano P, Papa MN (2017) Effects of climate change on shallow landslides in a small coastal catchment in southern Italy. Landslides 14:1043–1055. https://doi.org/10.1007/s10346-016-0743-1
19. Loye A, Jaboyedoff M, Pedrazzini A (2009) Identification of potential rockfall source areas at a regional scale using a DEM-based geomorphometric analysis. Nat. Hazards Earth Syst. Sci. 9:1643–1653. https://doi.org/10.5194/nhess-9-1643-2009
20. Ma S, Xu C, Shao X, Zhang P, Liang X, Tian Y (2019) Geometric and kinematic features of a landslide in Mabian Sichuan, China, derived from UAV photography. Landslides 16:373–381. https://doi.org/10.1007/s10346-018-1104-z
21. Wang, X., Liu, H., Sun, J., 2021. A new approach for identification of potential rockfall source areas controlled by rock mass strength at a regional scale. Remote Sens., 13(5), 938; https://doi.org/10.3390/rs13050938.
22. Qi S, Xu Q, Lan H, Zhang B, Liu J (2010) Spatial distribution analysis of landslides triggered by 2008.5.12 Wenchuan Earthquake, China. Engineering Geology 116:95–108. https://doi.org/10.1016/j.enggeo.2010.07.011
23. Stoffel M, Butler DR, Corona C (2013) Mass movements and tree rings: A guide to dendrogeomorphic field sampling and dating. Geomorphology 200:106–120. https://doi.org/10.1016/j.geomorph.2012.12.017
24. Stokes MA, Smiley TL (1968) An introduction to tree-ring dating. University of Arizona Press.
25. Cook ER, Kairiukstis LA (1990) Methods of Dendrochronology: Applications in the Environmental Sciences. Kluwer Academic Publishers, Dorefrecht.
26. Grissino-Mayer HD (2001) Evaluating crossdating accuracy- a manual and tutorial for the computer program COFECHA. Tree-Ring research 2:205–221
27. Ouyang C, He S, Xu Q, Luo Y, Zhang W (2013) A MacCormack-TVD finite difference method to simulate the mass flow in mountainous terrain with variable computational domain. Computers & Geosciences 52:1–10. https://doi.org/10.1016/j.cageo.2012.08.024
28. Iverson RM, Ouyang C (2015) Entrainment of bed material by Earth-surface mass flows: Review and reformulation of depth-integrated theory. Rev. Geophys. 53:27–58. https://doi.org/10.1002/2013RG000447
29. Ouyang C, Zhou K, Xu Q, Yin J, Peng D, Wang D, Li W (2017) Dynamic analysis and numerical modeling of the 2015 catastrophic landslide of the construction waste landfill at Guangming, Shenzhen, China. Landslides 14:705–718. https://doi.org/10.1007/s10346-016-0764-9
30. Sun J, Wang X, Liu H, Yuan H (2021) Effects of the attitude of dominant joints on the mobility of translational landslides. Landslides 18:2483–2498. https://doi.org/10.1007/s10346-021-01668-8
31. Van Den Eeckhaut M, Muys B, van Loy K, Poesen J, Beeckman H (2009) Evidence for repeated re-activation of old landslides under forest. Earth Surf. Process. Landforms 34:352–365. https://doi.org/10.1002/esp.1727
32. Ouyang C, Wang Z, An H, Liu X, Wang D (2019) An example of a hazard and risk assessment for debris flows—A case study of Niwan Gully, Wudu, China, Engineering Geology, 263:105351. https://10.1016/j.enggeo.2019.105351
33. Brang P (2001) Resistance and elasticity: promising concepts for the management of protection forests in the European Alps. Forest Ecology and Management 145:107–119. https://doi.org/10.1016/S0378-1127(00)00578-8
34. Wang X, Frattini P, Crosta GB, Zhang L, Agliardi F, Lari S, Yang Z (2014) Uncertainty assessment in quantitative rockfall risk assessment. Landslides 11:711–722. https://doi.org/10.1007/s10346-013-0447-8